Shupeng Li
Department of Mechanical Engineering,
Northwestern University,
Evanston, IL 60208
e-mail: shupengli2024@u.northwestern.edu

Yoonseok Park
Querrey Simpson Institute for Bioelectronics,
Northwestern University,
Evanston, IL 60208
e-mail: yoonseok.park@northwestern.edu

Haiwen Luan
Department of Mechanical Engineering,
Querrey Simpson Institute for Bioelectronics,
Northwestern University,
Evanston, IL 60208
e-mail: haiwenluan@u.northwestern.edu

Heling Wang
Department of Civil and Environmental Engineering,
Northwestern University,
Evanston, IL 60208
e-mail: helingwang1@gmail.com

Kyeongha Kwon
School of Electrical Engineering,
Korea Advanced Institute of Science and Technology,
Daejeon 34141, South Korea
e-mail: kyeonghaha@gmail.com

John A. Rogers[1]
Department of Materials Science and Engineering, Biomedical Engineering, Chemistry, Mechanical Engineering, Electrical and Computer Engineering, Neurological Surgery,
Querrey Simpson Institute for Bioelectronics,
Northwestern University,
Evanston, IL 60208
e-mail: jrogers@northwestern.edu

Yonggang Huang[1]
Department of Mechanical Engineering, Civil and Environmental Engineering, Materials Science and Engineering,
Querrey Simpson Institute for Bioelectronics,
Northwestern University,
Evanston, IL 60208
e-mail: y-huang@northwestern.edu

Measurement of Blood Pressure via a Skin-Mounted, Non-Invasive Pressure Sensor

Traditional methods to measure blood pressure are intermittent and may fail to detect the critical blood pressure fluctuations. Continuous blood pressure monitoring offers important clinical value in predicting cardiovascular diseases. Invasive (i.e., artery cannulation) and noninvasive approaches (e.g., volume clamping, pressure sensor, ultrasound, and optical methods) have limitations that prevent their generalized use outside of controlled settings, and few account properly for changes in the properties of the arteries (e.g., after drug administration, aging). This article proposes a method that combines a skin-interfaced pressure sensor with a sensor of pulse wave velocity, to continuously, noninvasively, and accurately measure the blood pressure, in ways that eliminate drifts and other artifacts that can prevent accurate, longitudinal monitoring. A scaling law is established to show that, for a linearly proportional relationship between the blood pressure and sensor pressure, the coefficient of proportionality depends on the elastic moduli E_{artery} and E_{tissue} of the artery and tissue, respectively, and the artery thickness h_{artery} and radius R_{artery} via a single, dimensionless combination, $E_{artery}h_{artery}/(E_{tissue}R_{artery})$, i.e., the normalized artery stiffness. This scheme determines the blood pressure in a manner that explicitly accounts for changes in the artery elastic modulus and thickness (e.g., due to the administration of drugs, aging). [DOI: 10.1115/1.4051183]

Keywords: blood pressure, pressure sensor, scaling law, pulse wave velocity

1 Introduction

Blood pressure (BP) represents a critically important vital sign for determining human health status. Both hypotension and hypertension are cardiovascular diseases that impair a range of basic bodily functions [1–3]. Continuous monitoring of BP yields streams of data that can be used to diagnose and predict health trajectories. Clinically, artery cannulation is considered to be the gold standard method of measuring BP [4]. This continuous and invasive way is highly accurate, but this invasiveness not only causes a variety of complications but also limits its application to hospital settings [5]. Hence, noninvasive measurements are attractive, typically classified into two categories: intermittent and continuous [6]. The former typically rely on an inflating cuff to measure BP manually (auscultatory and palpatory methods [7]) or automatically (oscillation method [8]). Differences between the cuff size and the circumference of the upper arm, the location of choice for these measurements can lead to inaccuracies [8]. Frequent cycles of inflation and deflation lead to repeated blockage of blood flow, with potential to cause discomfort as well as damage to the tissues [9]. Recent work defines several methods for continuous,

[1]Corresponding authors.

Contributed by the Applied Mechanics Division of ASME for publication in the Journal of Applied Mechanics. Manuscript received April 27, 2021; final manuscript received May 7, 2021; published online June 8, 2021. Assoc. Editor: Pradeep Sharma.

noninvasive measurements based on volume clamping [10,11], pressure sensors [12–23] (classic tonometry, piezoelectric, capacitive, resistive, or electronic skin), ultrasound [24,25], and optical [26–31] (photoplethysmography or pulse wave velocity [PWV]) methods. The volume clamping [10,11] and pressure sensor methods [12,13,17] measure BP on the finger or wrist accurately, but require bulky devices. The ultrasound techniques [24,25] are highly sensitive to motion artifacts and mostly involve heavy, bulky probes. Optical schemes [26–31] can be performed with small, comfortable devices, but they are highly susceptible to environmental factors [32] and/or changes in the blood composition [33]. All of these methods assume that the properties of the artery remain constant throughout the monitoring period and therefore yield results that vary due to pharmacological scheduling [34–36] and during long-term tracking (due to aging).

An alternative means to measure BP noninvasively and continuously exploits a soft, skin-interfaced pressure sensor [37,38], based on a cross-shape 3D structure encapsulated in a low modulus elastomer via a mechanics-guided three-dimensional (3D) assembly technique [39–52]. This type of small, flexible, wireless pressure sensor can operate accurately across a wide range of pressures with high accuracy and sensitivity [53]. This sensor creates advanced opportunities in BP measurement, as introduced here.

This article establishes a scaling law between the BP in the radial artery and the response of the pressure sensor via the finite element analysis (FEA), including explicitly the geometries and materials parameters of the artery and its surrounding tissue. The result provides the theoretical foundation for continuous measuring of BP. Together with separate measurements of PWV, this sensor can account for the effect of artery elastic modulus and thickness changes (e.g., due to drugs). Since the response of the pressure sensor and the PWV values can be both embodied in skin-interfaced wearable formats, this proposed method may lead to important opportunities for noninvasive, long-term, continuous, and accurate BP monitoring.

2 Model

As shown in Fig. 1(*a*), the setup includes a pressure sensor attached to the skin, directly above the radial artery. The pressure sensor and tissue are wrapped by an elastic band such as a wrist band. Figures 1(*b*) and 1(*c*) show the 3D model of the sensor, tissue and artery, where the sensor is rigid (since it is much stiffer than the tissue), and the artery (elastic modulus E_{artery}, thickness h_{artery}, external radius R_{artery}) is embedded in the tissue (elastic modulus E_{tissue}) at a depth d_{artery} (from the center of the artery) below the free surface (Fig. 1(*c*)). The bones (inside the tissue; Fig. 1(*a*)) are also modeled as rigid.

Let z axis denote the direction of the artery and y be the normal direction of the free surface (Figs. 1(*b*) and 1(*c*)). The tissue (Figs. 1(*b*) and 1(*c*)) has traction-free surfaces except that (1) the bottom surface, bonded to the bone, has vanishing displacements; (2) the two surfaces normal to the artery have vanishing normal (z) displacements such that the artery is not significantly stretched along its axial direction; and (3) the tissue and pressure sensor satisfy the continuity conditions across their interface, and the top surface of the sensor has vanishing normal (y) displacement to reflect the constraint effect of the elastic band.[2] This constraint yields a pressure on the sensor, P_{sensor}, due to the blood pressure BP applied inside the artery. For the linear elastic tissue and artery, the linear relation between P_{sensor} and BP is the focus of this article.

Two additional parameters involved in the analysis (Fig. 1(*c*)) are the spacing between the center of the artery and bone, d_{bone}, and sensor contact area with the tissue, S_{contact}. The in-plane (x and z directions) size of the tissue is much larger than d_{artery}, d_{bone}, and sensor size $\sqrt{S_{\text{contact}}}$ and therefore can be modeled as infinite.

The FEA via the commercial software ABAQUS is used to study the linear relation between P_{sensor} and BP. The eight-node linear brick, hybrid elements (C3D8RH) with the reduced integration is adopted, and the FEA mesh refinement ensures the accuracy of the simulations.

3 Results

Figure 2(*a*) shows the sensor pressure P_{sensor} versus the blood pressure BP for some combinations of the normalized artery modulus $E_{\text{artery}}/E_{\text{tissue}}$ (=2.5, 5, 17 and 34) and artery thickness $h_{\text{artery}}/R_{\text{artery}}$ (=0.095, 0.19, and 0.28). The baseline values of other parameters are the normalized artery depth to the free surface $d_{\text{artery}}/R_{\text{artery}} = 2.9$ [33,54] and to the bone $d_{\text{bone}}/d_{\text{artery}} = 1$, and sensor contact area $S_{\text{contact}}/R_{\text{artery}}^2 = 9.6$. As expected, Fig. 2(*a*) shows a linear relation:[3]

$$\text{BP} = kP_{\text{sensor}} \tag{1}$$

where the dimensionless factor k depends on the modulus ratio and other normalized parameters from Fig. 1(*c*) as follows:

$$k = k\left(\frac{E_{\text{artery}}}{E_{\text{tissue}}}, \frac{h_{\text{artery}}}{R_{\text{artery}}}, \frac{d_{\text{artery}}}{R_{\text{artery}}}, \frac{d_{\text{bone}}}{d_{\text{artery}}}, \frac{S_{\text{contact}}}{R_{\text{artery}}^2}\right) \tag{2}$$

The straight line for $E_{\text{artery}}/E_{\text{tissue}} = 5$ and $h_{\text{artery}}/R_{\text{artery}} = 0.095$ in Fig. 2(*a*) coincides with the line for (half of the artery modulus value) $E_{\text{artery}}/E_{\text{tissue}} = 2.5$ and (double the artery thickness value) $h_{\text{artery}}/R_{\text{artery}} = 0.19$, which suggests that the dependence of the factor k on the artery modulus E_{artery} and thickness h_{artery} is through their product $E_{\text{artery}}h_{\text{artery}}$, i.e., through the normalized arterial tensive stiffness $\frac{E_{\text{artery}}h_{\text{artery}}}{E_{\text{tissue}}R_{\text{artery}}}$. This is confirmed for another pair elastic modulus and thickness in Fig. 2(*a*), ($E_{\text{artery}}/E_{\text{tissue}}$, $h_{\text{artery}}/R_{\text{artery}}$) = (34, 0.095) and (17, 0.19). Figure 2(*b*) shows that the factor k versus $\frac{E_{\text{artery}}h_{\text{artery}}}{E_{\text{tissue}}R_{\text{artery}}}$ for wide ranges of artery modulus $E_{\text{artery}}/E_{\text{tissue}}$ (2.5∼34) and thickness $h_{\text{artery}}/R_{\text{artery}}$ (0.095–0.28), which are wide enough to cover the relevant ranges for humans. The $k \sim \frac{E_{\text{artery}}h_{\text{artery}}}{E_{\text{tissue}}R_{\text{artery}}}$ relation in Fig. 2(*b*) is approximately linear, i.e.,

$$k = f\frac{E_{\text{artery}}h_{\text{artery}}}{E_{\text{tissue}}R_{\text{artery}}} \tag{3}$$

where f is the slope of the line in Fig. 3(*b*), and it depends on

$$f = f\left(\frac{d_{\text{artery}}}{R_{\text{artery}}}, \frac{d_{\text{bone}}}{d_{\text{artery}}}, \frac{S_{\text{contact}}}{R_{\text{artery}}^2}\right) \tag{4}$$

The linear relation between k and $\frac{E_{\text{artery}}h_{\text{artery}}}{E_{\text{tissue}}R_{\text{artery}}}$ in Eq. (3) is confirmed in Figs. 3(*a*), 3(*c*), and 3(*e*) for wide ranges of $d_{\text{artery}}/R_{\text{artery}}$, $d_{\text{bone}}/d_{\text{artery}}$, and $S_{\text{contact}}/R_{\text{artery}}^2$, respectively. The baseline values are $E_{\text{artery}}/E_{\text{tissue}} = 7.7$ [55,56], $h_{\text{artery}}/R_{\text{artery}} = 0.19$ [56–58], and other parameters shown earlier. Figures 3(*b*), 3(*d*), and 3(*f*) further show that the slope f in Eq. (3) increases with $d_{\text{artery}}/R_{\text{artery}}$, $d_{\text{bone}}/d_{\text{artery}}$, and $S_{\text{contact}}/R_{\text{artery}}^2$, respectively.

[2]The constraint effect of the elastic band will be further discussed in the later sections.

[3]The pressure sensor may have an initial reading P_{sensor0} in the absence of BP, due to the over constraint of the elastic stiff, such that Eq. (1) becomes $\text{BP} = k(P_{\text{sensor}} - P_{\text{sensor0}})$. Its implication on the BP measurement will be discussed in later sections.

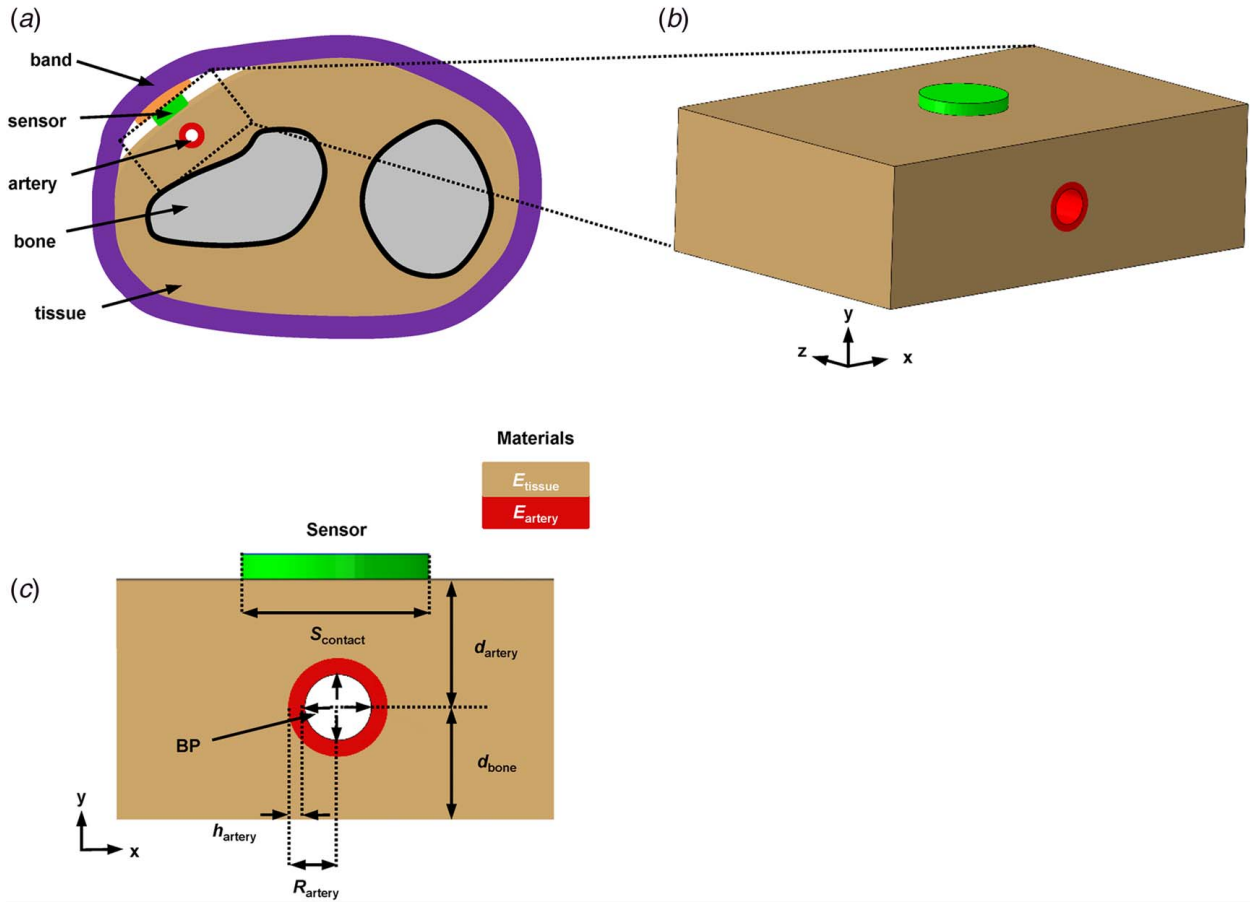

Fig. 1 (*a*) Schematic cross-sectional view of a radial artery in a tissue with a pressure sensor, (*b*) a 3D model for the sensor, tissue, and artery, and (*c*) cross-sectional view of the 3D model with all parameters labeled

4 Application to Blood Pressure Measurement

The linear proportionality between BP and P_{sensor} in Eq. (1) provides a simple means to determine the blood pressure. However, its coefficient of proportionality k, even though studied thoroughly in the prior sections, depends on many parameters (e.g., E_{artery}, h_{artery}, R_{artery}, d_{artery}, d_{bone}, and E_{tissue}) that are inaccessible (difficult to measure) as they vary not only between individuals but also across different locations for a given person. Therefore, the most effective way is to calibrate k in a laboratory or clinic setting, i.e., by measuring the blood pressure $(BP)_{lab}$ (via the methods discussed in Sec. 1) and sensor pressure $(P_{sensor})_{lab}$ simultaneously in a lab, which yields $k_{lab} = (BP)_{lab}/(P_{sensor})_{lab}$. If one assumes the artery properties remain constant, i.e., k remains the same, then Eq. (1) becomes

$$BP = k_{lab} P_{sensor} \tag{5}$$

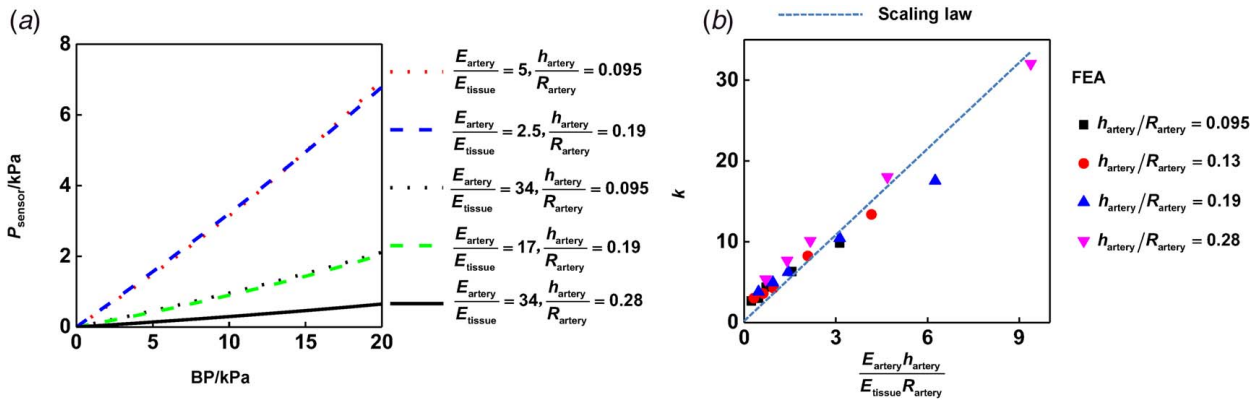

Fig. 2 (*a*) Linear relation between the sensor pressure and the blood pressure for a wide range of the artery modulus and thickness and (*b*) the reciprocal of the slope in (*a*), k, versus the normalized artery stiffness $E_{artery}h_{artery}/(E_{tissue}R_{artery})$ for a wide range of artery-to-tissue modulus ratio and thickness-to-radius ratio of the artery, and the normalized distances from the center of the artery to the free surface $d_{artery}/R_{artery} = 2.9$, to the bone $d_{bone}/d_{artery} = 1$, and contact area of the sensor $S_{contact}/R_{artery}^2 = 9.6$

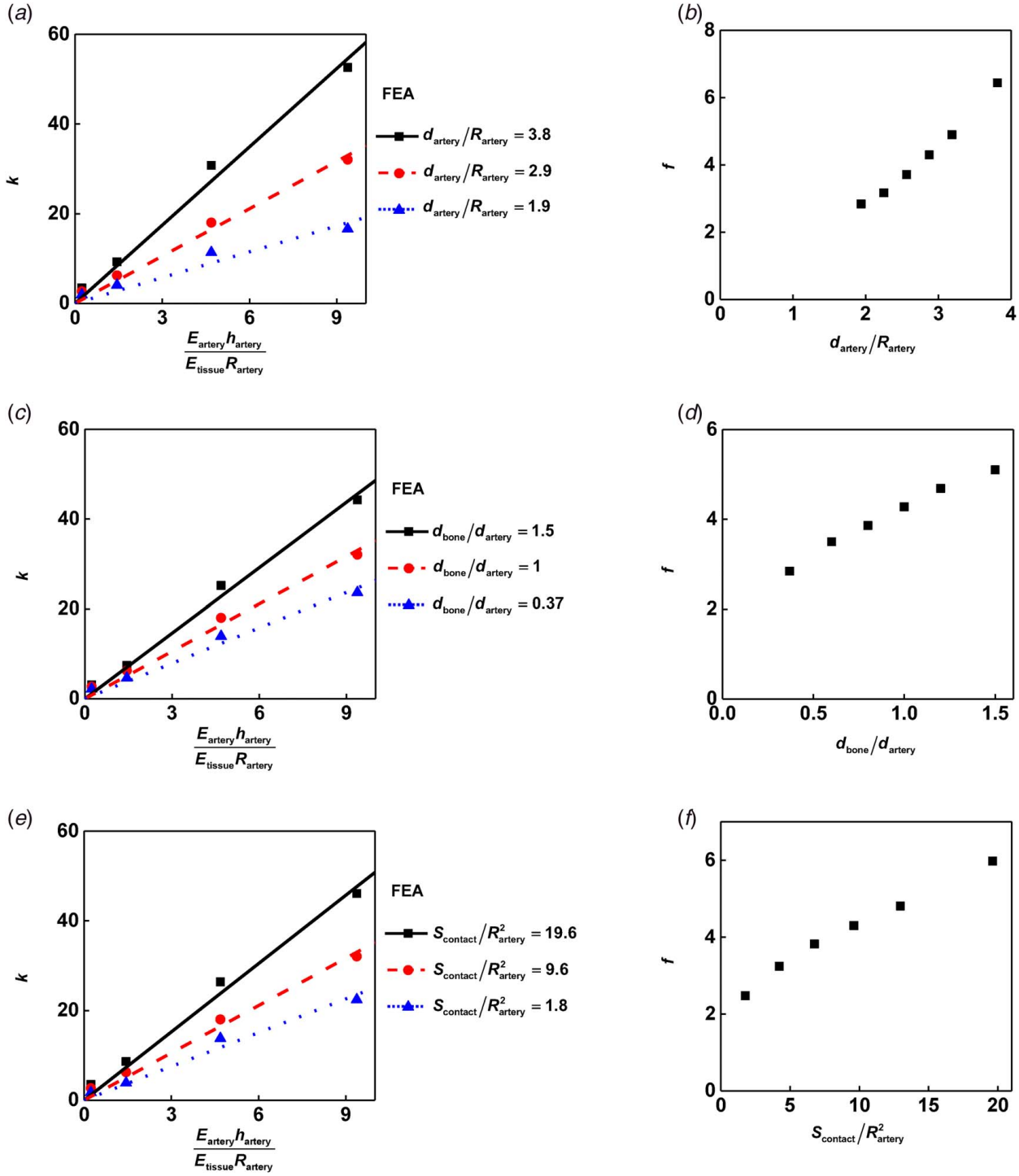

Fig. 3 The coefficient k of linear proportionality (between BP and sensor pressure P_{sensor}) versus the normalized artery stiffness $E_{artery}h_{artery}/(E_{tissue}R_{artery})$ for various values of (*a*) the normalized depth to the free surface d_{artery}/R_{artery}, (*c*) the normalized distance to the bone d_{bone}/d_{artery}, and (*e*) the normalized sensor contact area $S_{contact}/R^2_{artery}$, which all suggest a linear relation $k = fE_{artery}h_{artery}/(E_{tissue}R_{artery})$; and the dependence of f on d_{artery}/R_{artery}, d_{bone}/d_{artery}, and $S_{contact}/R^2_{artery}$ in (*b*), (*d*), and (*f*), respectively, for the same baseline values as in Fig. 2

This suggestion of determining BP via the pressure sensor is particularly suitable outside the laboratory or clinic setting where the existing methods (e.g., those discussed in Sec. 1) are unavailable. For Eq. (5) to hold, the pressure sensor must be placed at the same location and the same elastic band being used for each person in different environments (e.g., in a lab, at home or outdoors) such that the local artery modulus, thickness, and other parameters all remain the same.

The artery elastic modulus and thickness, however, may change, such as after the drugs are administered [34–36], or due to aging. These changes not only influence the BP itself but also alter the value of k, which depends on E_{artery} and h_{artery}, different from k_{lab} such that Eq. (5) no long holds. The method proposed earlier is modified in the following to combine the pressure sensor and PWV measurement to account for the artery elastic modulus and thickness changes. The well-known Moens–Korteweg equation

[59] gives $\mathrm{PWV} = \sqrt{\frac{E_{\mathrm{artery}} h_{\mathrm{artery}}}{2R_{\mathrm{artery}}\rho_{\mathrm{blood}}}}$, where ρ_{blood} is the mass density of blood. Therefore, changes in the artery modulus and thickness of a patient can be reflected in the change in PWV. The factor k between BP and P_{sensor} can be written in terms of the PWV as follows:

$$k = f\frac{2\rho_{\mathrm{blood}}}{E_{\mathrm{tissue}}}\mathrm{PWV}^2 \tag{6}$$

Under the reasonable assumption that the blood mass density ρ_{blood}, tissue modulus E_{tissue}, artery outer radius R_{artery}, and depths d_{artery} to the free surface and d_{bone} to the bone do not change substantially due to the drugs, the above equation can be rewritten as

$$k = k_{\mathrm{lab}}\left(\frac{\mathrm{PWV}}{\mathrm{PWV}_{\mathrm{lab}}}\right)^2 \tag{7}$$

where $\mathrm{PWV}_{\mathrm{lab}}$ is the pulse wave velocity measured in the lab, simultaneously with k_{lab}. Equations (1) and (7) then establish the method to determine BP via the pressure sensor and PWV measurement. Here, the pressure sensor and PWV measurement must be placed at the same location for each person.

5 Discussion and Concluding Remarks

A few points on the model, particularly its application to measure the blood pressure, are presented.

(1) *Initial sensor pressure unrelated to BP*: As shown in Fig. 1(*a*), the pressure sensor is pressed into the tissue by an elastic band. This arrangement may yield an initial sensor pressure, P_{sensor0}, in the absence of any BP such that Eq. (1) can be modified as $\mathrm{BP} = k(P_{\mathrm{sensor}} - P_{\mathrm{sensor0}})$, or via the change of blood pressure $\Delta\mathrm{BP}$ and change of sensor pressure $\Delta P_{\mathrm{sensor}}$ as follows:

$$\Delta\mathrm{BP} = k\Delta P_{\mathrm{sensor}} \tag{8}$$

speaking, the slope k in Eq. (8) may depend on the stiffness of the elastic band, i.e., pressing the sensor into the tissue may deform the artery and therefore changes k. The FEA results show that the linear relation in Eq. (8) still holds, and the resulting k is still linearly proportion to $\frac{E_{\mathrm{artery}} h_{\mathrm{artery}}}{E_{\mathrm{tissue}} R_{\mathrm{artery}}}$ as in Eq. (3), even for the initial sensor pressure P_{sensor0} as large as 160 kPa, which corresponds to the sensor being pressed into the tissue almost as deep as the radius of the artery. In addition, the same elastic band should be used, for both the calibration in the lab and applications, to ensure the same k.

(2) *Linear elasticity for human arteries*: The aforementioned analysis is based on linear elasticity of the human arteries, which, in general, are hyper-elastic [60–62]. For the human artery parameters [60,61] and the normal range of blood pressure from ~9 kPa to 16 kPa (or ~70–120 mmHg), the numerical results suggest that the incremental linear relation in Eq. (8) still holds, though k depends on the instantaneous (tangent) modulus, rather than the initial modulus, of the artery.

(3) *Why k is linearly proportional to the artery stiffness?* Even though the linear relation in Eq. (3) between the coefficient of proportionality k (between P_{sensor} and BP) and the normalized artery stiffness $E_{\mathrm{artery}}h_{\mathrm{artery}}/(E_{\mathrm{tissue}}R_{\mathrm{artery}})$ is discovered from the FEA results, a clear mechanics explanation exists. As the artery expands due to BP, the artery wall is mainly stretched in the circumferential direction such that its deformation is influenced by the tensile stiffness $E_{\mathrm{artery}}h_{\mathrm{artery}}$, rather than bending stiffness, for the case of a relatively thin artery wall. For a thick artery wall $h_{\mathrm{artery}}/R_{\mathrm{artery}} = 0.44$, which corresponds to the artery wall occupying 69% of the cross-sectional area of the artery (i.e., leaving only 31% of the cross-sectional area for blood flow), the FEA results show that the error in Eq. (3) is as large as 47%, i.e., k depends on E_{artery} and h_{artery} individually, rather than through the tensile stiffness $E_{\mathrm{artery}}h_{\mathrm{artery}}$. In addition, for a given value of BP, the linear elasticity theory suggests that the deformation is inversely proportional to the elastic modulus E_{artery}, which suggests $P_{\mathrm{sensor}} \propto 1/E_{\mathrm{artery}}$, leading to $k \propto E_{\mathrm{artery}}$ (therefore, $k \propto E_{\mathrm{artery}}h_{\mathrm{artery}}$).

(4) *Sensor shape and position*: The FEA results presented earlier are based on a circular sensor, but the proposed method still works for other shapes of the sensor, as long as the same sensor is used in both calibration in the lab and applications. The FEA results also suggest that the proposed method is insensitive to the position of the sensor on the tissue. For example, for the centers of the sensor and artery do not line up, the value of k (also f in Eq. (3)) remains almost same even for the offset distance between two centers as large as the artery radius (i.e., the center of the sensor is directly above the edge, instead of the center, of the artery).

In summary, this article presents a method that accounts for changes in arterial properties change in noninvasive, continuous measurements of BP via a combination of a pressure sensor and measurement of pulse wave velocity. The results establish that the BP is linearly proportional to the sensor pressure as the sensor is placed on the skin, and the coefficient of proportionality scales linearly with the artery stiffness. As the PWV is directly related to the artery stiffness, combining the output of the pressure sensor with a measurement of PWV serves as the basis for conveniently monitor the BP with potential applicability in the home, continuously over long time, even accounting for any changes in the artery modulus and thickness.

Conflict of Interest

There are no conflicts of interest.

Data Availability Statement

The datasets generated and supporting the findings of this article are obtainable from the corresponding author upon reasonable request. The authors attest that all data for this study are included in the paper.

References

[1] Bijker, J. B., Persoon, S., Peelen, L. M., Moons, K. G., Kalkman, C. J., Kappelle, L. J., and Van Klei, W. A., 2012, "Intraoperative Hypotension and Perioperative Ischemic Stroke After General Surgery: A Nested Case-Control Study," Anesthesiology, **116**(3), pp. 658–664.

[2] van Waes, J. A., Van Klei, W. A., Wijeysundera, D. N., Van Wolfswinkel, L., Lindsay, T. F., and Beattie, W. S., 2016, "Association Between Intraoperative Hypotension and Myocardial Injury After Vascular Surgery," Anesthesiology, **124**(1), pp. 35–44.

[3] Walsh, M., Devereaux, P. J., Garg, A. X., Kurz, A., Turan, A., Rodseth, R. N., Cywinski, J., Thabane, L., and Sessler, D. I., 2013, "Relationship Between Intraoperative Mean Arterial Pressure and Clinical Outcomes After Noncardiac Surgery: Toward an Empirical Definition of Hypotension," Anesthesiology, **119**(3), pp. 507–515.

[4] Saugel, B., Dueck, R., and Wagner, J. Y., 2014, "Measurement of Blood Pressure," Best Pract. Res. Clin. Anaesthesiol., **28**(4), pp. 309–322.

[5] Scheer, B. V., Perel, A., and Pfeiffer, U. J., 2002, "Clinical Review: Complications and Risk Factors of Peripheral Arterial Catheters Used for Haemodynamic Monitoring in Anaesthesia and Intensive Care Medicine," Crit. Care, **6**(3), pp. 1–7.

[6] Meidert, A. S., and Saugel, B. J., 2018, "Techniques for Non-Invasive Monitoring of Arterial Blood Pressure," Front. Med., **4**, p. 231.

[7] Liu, S., and Wan, K., 2019, "A Preliminary Two-Dimensional Palpation Mechanics for Detecting a Hard Inclusion by Indentation of a Soft Matrix Under Large Strain," ASME J. Appl. Mech., **86**(5), p. 051009.

[8] Bur, A., Hirschl, M. M., Herkner, H., Oschatz, E., Kofler, J., Woisetschläger, C., and Laggner, A. N., 2000, "Accuracy of Oscillometric Blood Pressure Measurement According to the Relation Between Cuff Size and Upper-Arm Circumference in Critically Ill Patients," Crit. Care Med., **28**(2), pp. 371–376.
[9] Pickering, T. G., Hall, J. E., Appel, L. J., Falkner, B. E., Graves, J., Hill, M. N., Jones, D. W., Kurtz, T., Sheps, S. G., and Roccella, E. J., 2005, "Recommendations for Blood Pressure Measurement in Humans and Experimental Animals: Part 1: Blood Pressure Measurement in Humans: A Statement for Professionals From the Subcommittee of Professional and Public Education of the American Heart Association Council on High Blood Pressure Research," Hypertension, **45**(1), pp. 142–161.
[10] Penaz, J., Voigt, A., and Teichmann, W., 1976, "Contribution to the Continuous Indirect Blood Pressure Measurement," Z. Gesamte Inn. Med., **31**(24), pp. 1030–1033.
[11] Wagner, J. Y., Grond, J., Fortin, J., Negulescu, I., Schöfthaler, M., and Saugel, B., 2016, "Continuous Noninvasive Cardiac Output Determination Using the CNAP System: Evaluation of a Cardiac Output Algorithm for the Analysis of Volume Clamp Method-Derived Pulse Contour," J. Clin. Monit. Comput., **30**(4), pp. 487–493.
[12] Pressman, G. L., and Newgard, P. M., 1963, "A Transducer for the Continuous External Measurement of Arterial Blood Pressure," IEEE Trans. Biomed. Circuits Syst., **10**(2), pp. 73–81.
[13] Dueck, R., Goedje, O., and Clopton, P., 2012, "Noninvasive Continuous Beat-to-Beat Radial Artery Pressure via TL-200 Applanation Tonometry," J. Clin. Monit. Comput., **26**(2), pp. 75–83.
[14] Schwartz, G., Tee, B. C.-K., Mei, J., Appleton, A. L., Kim, D. H., Wang, H., and Bao, Z., 2013, "Flexible Polymer Transistors With High Pressure Sensitivity for Application in Electronic Skin and Health Monitoring," Nat. Commun., **4**(1), pp. 1–8.
[15] Dagdeviren, C., Su, Y., Joe, P., Yona, R., Liu, Y., Kim, Y.-S., Huang, Y., Damadoran, A. R., Xia, J., Martin, L. W., Huang, Y., and Rogers, J. A., 2014, "Conformable Amplified Lead Zirconate Titanate Sensors With Enhanced Piezoelectric Response for Cutaneous Pressure Monitoring," Nat. Commun., **5**(1), pp. 1–10.
[16] Kim, J., Chou, E. F., Le, J., Wong, S., Chu, M., and Khine, M., 2019, "Soft Wearable Pressure Sensors for Beat-to-Beat Blood Pressure Monitoring," Adv. Healthcare Mater., **8**(13), p. 1900109.
[17] Panula, T., Koivisto, T., Pänkäälä, M., Niiranen, T., Kantola, I., and Kaisti, M., 2020, "An Instrument for Measuring Blood Pressure and Assessing Cardiovascular Health From the Fingertip," Biosens. Bioelectron., **167**, p. 112483.
[18] Huang, Y.-C., Liu, Y., Ma, C., Cheng, H.-C., He, Q., Wu, H., Wang, C., Lin, C.-Y., Huang, Y., and Duan, X., 2020, "Sensitive Pressure Sensors Based on Conductive Microstructured Air-Gap Gates and Two-Dimensional Semiconductor Transistors," Nat. Electron., **3**(1), pp. 59–69.
[19] Chu, Y., Zhong, J., Liu, H., Ma, Y., Liu, N., Song, Y., Liang, J., Shao, Z., Sun, Y., Dong, Y., Wang, X., and Lin, L.,2018, "Human Pulse Diagnosis for Medical Assessments Using a Wearable Piezoelectret Sensing System," Adv. Funct. Mater., **28**(40), p. 1803413.
[20] Zou, B., Chen, Y., Liu, Y., Xie, R., Du, Q., Zhang, T., Shen, Y., Zheng, B., Li, S., Wu, J., Zhang, W., Huang, W., Huang, X., and Huo, F., 2019, "Repurposed Leather With Sensing Capabilities for Multifunctional Electronic Skin," Adv. Sci., **6**(3), p. 1801283.
[21] Meng, K., Zhao, S., Zhou, Y., Wu, Y., Zhang, S., He, Q., Wang, X., Zhou, Z., Fan, W., Tan, X., Yang, J., and Chen, J., 2020, "A Wireless Textile-Based Sensor System for Self-Powered Personalized Health Care," Matter, **2**(4), pp. 896–907.
[22] Peng, X., Dong, K., Ye, C., Jiang, Y., Zhai, S., Cheng, R., Liu, D., Gao, X., Wang, J., and Wang, Z. L., 2020, "A Breathable, Biodegradable, Antibacterial, and Self-Powered Electronic Skin Based on All-Nanofiber Triboelectric Nanogenerators," Sci. Adv., **6**(26), p. eaba9624.
[23] Zhang, Y., Lü, C., Lu, B., Feng, X., and Wang, J., 2020, "Theoretical Modeling on Monitoring Left Ventricle Deformation Using Conformal Piezoelectric Sensors," ASME J. Appl. Mech., **87**(1), p. 011007.
[24] Wang, C., Li, X., Hu, H., Zhang, L., Huang, Z., Lin, M., Zhang, Z., Yin, Z., Huang, B., Gong, H., Bhaskaran, S., Gu, Y., Makihata, M., Guo, Y., Lei, Y., Chen, Y., Wang, C., Yang, L., Zhang, T., Chen, Z., Pisano, A. P., Zhang, L., Zhou, Q., and Xu, S., 2018, "Monitoring of the Central Blood Pressure Waveform via a Conformal Ultrasonic Device," Nat. Biomed. Eng., **2**(9), pp. 687–695.
[25] Howard, G., Sharrett, A. R., Heiss, G., Evans, G. W., Chambless, L. E., Riley, W. A., and Burke, G. L., 1993, "Carotid Artery Intimal-Medial Thickness Distribution in General Populations as Evaluated by B-Mode Ultrasound. ARIC Investigators," Stroke, **24**(9), pp. 1297–1304.
[26] Kim, J., Salvatore, G. A., Araki, H., Chiarelli, A. M., Xie, Z., Banks, A., Sheng, X., Liu, Y., Lee, J. W., Jang, K.-I., Heo, S. Y., Cho, K., Luo, H., Zimmerman, B., Kim, J., Yan, L., Feng, X., Xu, S., Fabiani, M., Gratton, G., Huang, Y., Paik, U., and Rogers, J. A., 2016, "Battery-Free, Stretchable Optoelectronic Systems for Wireless Optical Characterization of the Skin," Sci. Adv., **2**(8), p. e1600418.
[27] Chandrasekhar, A., Kim, C.-S., Naji, M., Natarajan, K., Hahn, J.-O., and Mukkamala, R., 2018, "Smartphone-Based Blood Pressure Monitoring via the Oscillometric Finger-Pressing Method," Sci. Transl. Med., **10**(431), p. eaap8679.
[28] Ma, Y., Choi, J., Hourlier-Fargette, A., Xue, Y., Chung, H. U., Lee, J. Y., Wang, X., Xie, Z., Kang, D., Wang, H., Han, S., Kang, S.-K., Kang, Y., Yu, X., Slepian, M. J., Raj, M. S., Model, J. B., Feng, X., Ghaffari, R., Rogers, J. A., and Huang, Y., 2018, "Relation Between Blood Pressure and Pulse Wave Velocity for Human Arteries," Proc. Natl. Acad. Sci. USA, **115**(44), pp. 11144–11149.
[29] Boutry, C. M., Nguyen, A., Lawal, Q. O., Chortos, A., Rondeau-Gagné, S., and Bao, Z., 2015, "A Sensitive and Biodegradable Pressure Sensor Array for Cardiovascular Monitoring," Adv. Mater., **27**(43), pp. 6954–6961.
[30] Katsuura, T., Izumi, S., Yoshimoto, M., Kawaguchi, H., Yoshimoto, S., and Sekitani, T., 2017, "Wearable Pulse Wave Velocity Sensor Using Flexible Piezoelectric Film Array," IEEE Biomedical Circuits and Systems Conference (BioCAS), Turin, Italy, Oct. 19–21, pp. 1–4.
[31] Jia, Y., Punithakumar, K., Noga, M., and Hemmati, A., 2021, "Blood Flow Manipulation in the Aorta With Coarctation and Arch Narrowing for Pediatric Subjects," ASME J. Appl. Mech., **88**(2), p. 021001.
[32] Maeda, Y., Sekine, M., and Tamura, T., 2011, "Relationship Between Measurement Site and Motion Artifacts in Wearable Reflected Photoplethysmography," J. Med. Syst., **35**(5), pp. 969–976.
[33] Melhuish, T. M., and White, L. D., 2016, "Optimal Wrist Positioning for Radial Arterial Cannulation in Adults: A Systematic Review and Meta-Analysis," Am. J. Emerg. Med., **34**(12), pp. 2372–2378.
[34] Bank, A. J., Wilson, R. F., Kubo, S. H., Holte, J. E., Dresing, T. J., and Wang, H., 1995, "Direct Effects of Smooth Muscle Relaxation and Contraction on in Vivo Human Brachial Artery Elastic Properties," Circ. Res., **77**(5), pp. 1008–1016.
[35] Bank, A. J., 1997, "Physiologic Aspects of Drug Therapy and Large Artery Elastic Properties," Vasc. Med., **2**(1), pp. 44–50.
[36] Jayendiran, R., Nour, B., and Ruimi, A., 2021, "Performance of a Nitinol Honeycomb Stent for the Management of Atherosclerotic Aortic Plaque: Crimping, Sealing, and Fluid–Structure Interaction Analysis," ASME J. Appl. Mech., **88**(3), p. 031013.
[37] Won, S. M., Wang, H., Kim, B. H., Lee, K., Jang, H., Kwon, K., Han, M., Crawford, K. E., Li, H., Lee, Y., Yuan, X., Kim, S. B., Oh, Y. S., Jang, W. J., Lee, J. Y., Han, S., Kim, J., Wang, X., Xie, Z., Zhang, Y., Huang, Y., and Rogers, J. A., 2019, "Multimodal Sensing With a Three-Dimensional Piezoresistive Structure," ACS Nano, **13**(10), pp. 10972–10979.
[38] Park, Y., Kwon, K., Kwak, S. S., Kwak, J. W., Luan, H., Chung, T. S., San Chun, K., Kim, J. U., Jang, H., Ryu, H., Jeong, H., Won, S. M., Kang, Y. J., Zhang, M., Pontes, D., Kampmeier, B. R., Seo, S. H., Zhao, J., Jung, I., Huang, Y., Xu, S., and Rogers, J. A., 2020, "Wireless, Skin-Interfaced Sensors for Compression Therapy," Sci. Adv., **6**(49), p. eabe1655.
[39] Xu, S., Yan, Z., Jang, K.-I., Huang, W., Fu, H., Kim, J., Wei, Z., Flavin, M., McCracken, J., Wang, R., Badea A, Liu, Y., Xiao, D., Zhou, G., Lee, J., Chung, H. U., Ren, W., Banks, A., Li, X., Paik, U., Nuzzo, R. G., Huang, Y., Zhang, Y., and Rogers, J. A., 2015, "Assembly of Micro/Nanomaterials Into Complex, Three-Dimensional Architectures by Compressive Buckling," Science, **347**(6218), pp. 154–159.
[40] Zhang, Y., Yan, Z., Nan, K., Xiao, D., Liu, Y., Luan, H., Fu, H., Wang, X., Yang, Q., Wang, J., Ren, W., Si, H., Liu, F., Yang, L., Li, H., Wang, J., Guo, X., Luo, H., Wang, L., Huang, Y., and Rogers, J. A., 2015, "A Mechanically Driven Form of Kirigami as a Route to 3D Mesostructures in Micro/Nanomembranes," Proc. Natl. Acad. Sci. USA, **112**(38), pp. 11757–11764.
[41] Yan, Z., Zhang, F., Liu, F., Han, M., Ou, D., Liu, Y., Lin, Q., Guo, X., Fu, H., Xie, Z., Gao, M., Huang, Y., Kim, J., Qiu, Y., Nan, K., Kim, J., Gutruf, P., Luo, H., Zhao, A., Hwang, K.-C., Huang, Y., Zhang, Y., and Rogers, J. A., 2016, "Mechanical Assembly of Complex, 3D Mesostructures From Releasable Multilayers of Advanced Materials," Sci. Adv., **2**(9), p. e1601014.
[42] Fu, H., Nan, K., Bai, W., Huang, W., Bai, K., Lu, L., Zhou, C., Liu, Y., Liu, F., Wang, J., Han, M., Yan, Z., Luan, H., Zhang, Y., Zhang, Y., Zhao, J., Xu, C., Li, M., Lee, J. W., Liu, Y., Fang, D., Li, X., Huang, Y., Zhang, Y., and Rogers, J. A., 2018, "Morphable 3D Mesostructures and Microelectronic Devices by Multistable Buckling Mechanics," Nat. Mater., **17**(3), pp. 268–276.
[43] Ning, X., Yu, X., Wang, H., Sun, R., Corman, R., Li, H., Lee, C. M., Xue, Y., Chempakasseril, A., Yao, Y., Zhang, Z., Luan, H., Wang, Z., Xia, W., Feng, X., Ewoldt, R. H., Huang, Y., Zhang, Y., and Rogers, J. A., 2018, "Mechanically Active Materials in Three-Dimensional Mesostructures," Sci. Adv., **4**(9), p. eaat8313.
[44] Han, M., Wang, H., Yang, Y., Liang, C., Bai, W., Yan, Z., Li, H., Xue, Y., Wang, X., Akar, B., Zhao, H., Luan, H., Lim, J., Kandela, I., Ameer, G. A., Zhang, Y., Huang, Y., and Rogers, J. A., 2019, "Three-Dimensional Piezoelectric Polymer Microsystems for Vibrational Energy Harvesting, Robotic Interfaces and Biomedical Implants," Nat. Electron., **2**(1), pp. 26–35.
[45] Zhu, F., Xiao, H., Li, H., Huang, Y., and Ma, Y., 2019, "Irregular Hexagonal Cellular Substrate for Stretchable Electronics," ASME J. Appl. Mech., **86**(3), p. 034501.
[46] Yan, Z., Wang, B., Wang, K., Zhao, S., Li, S., Huang, Y., and Wang, H., 2020, "Cellular Substrate to Facilitate Global Buckling of Serpentine Structures," ASME J. Appl. Mech., **87**(2), p. 024501.
[47] Xu, Z., Fan, Z., Zi, Y., Zhang, Y., and Huang, Y., 2020, "An Inverse Design Method of Buckling-Guided Assembly for Ribbon-Type 3D Structures," ASME J. Appl. Mech., **87**(3), p. 031004.
[48] Li, K., Chen, L., Zhu, F., and Huang, Y., 2021, "Thermal and Mechanical Analyses of Compliant Thermoelectric Coils for Flexible and Bio-Integrated Devices," ASME J. Appl. Mech., **88**(2), p. 021011.
[49] Yin, S., and Su, Y., 2019, "A Traction-Free Model for the Tensile Stiffness and Bending Stiffness of Laminated Ribbons of Flexible Electronics," ASME J. Appl. Mech., **86**(5), p. 051011.
[50] Feng, P., Yuan, J., Huang, Y., and Li, X., 2020, "Analytical Solutions for the Lateral-Torsional Buckling of Serpentine Interconnects in Stretchable Electronics," ASME J. Appl. Mech., **87**(8), p. 081005.
[51] Liu, G., Sun, L., and Su, Y., 2020, "Scaling Effects in the Mechanical System of the Flexible Epidermal Electronics and the Human Skin," ASME J. Appl. Mech., **87**(8), p. 081007.

[52] Zhao, S., Zhu, F., Yan, Z., Li, D., Xiang, J., Huang, Y., and Luan, H., 2020, "A Nonlinear Mechanics Model of Zigzag Cellular Substrates for Stretchable Electronics," ASME J. Appl. Mech., **87**(6), p. 061006.
[53] Yuan, X., Won, S. M., Han, M., Wang, Y., Rogers, J. A., Huang, Y., and Wang, H., 2021, "Mechanics of Encapsulated Three-Dimensional Structures for Simultaneous Sensing of Pressure and Shear Stress," J. Mech. Phys. Solids, **151**, p. 104400.
[54] Kim, J. U., Lee, Y. J., Lee, J., and Kim, J. Y., 2015, "Differences in the Properties of the Radial Artery Between cun, Guan, chi, and Nearby Segments Using Ultrasonographic Imaging: A Pilot Study on Arterial Depth, Diameter, and Blood Flow," Evidence-Based Complementary Altern. Med., **2015**, p. 381634.
[55] Singh, P., Choudhury, M. I., Roy, S., and Prasad, A., 2017, "Computational Study to Investigate Effect of Tonometer Geometry and Patient-Specific Variability on Radial Artery Tonometry," J. Biomech., **58**, pp. 105–113.
[56] Laurent, S., Girerd, X., Mourad, J.-J., Lacolley, P., Beck, L., Boutouyrie, P., Mignot, J.-P., and Safar, M., 1994, "Elastic Modulus of the Radial Artery Wall Material Is Not Increased in Patients With Essential Hypertension," Arterioscler. Thromb. Vasc. Biol., **14**(7), pp. 1223–1231.
[57] Riley, W. A., Barnes, R. W., Evans, G. W., and Burke, G. L., 1992, "Ultrasonic Measurement of the Elastic Modulus of the Common Carotid Artery. The Atherosclerosis Risk in Communities (ARIC) Study," Stroke, **23**(7), pp. 952–956.
[58] Girerd, X., Giannattasio, C., Moulin, C., Safar, M., Mancia, G., and Laurent, S., 1998, "Regression of Radial Artery Wall Hypertrophy and Improvement of Carotid Artery Compliance After Long-Term Antihypertensive Treatment in Elderly Patients," J. Am. Coll. Cardiol., **31**(5), pp. 1064–1073.
[59] Bramwell, J. C., and Hill, A. V., "Containing Papers of a Biological Character, 1922, "The Velocity of Pulse Wave in Man," Proc. R. Soc. Lond. B., **93**(652), pp. 298–306.
[60] Fung, Y.-C., 2013, *Biomechanics: Circulation*, Springer Science & Business Media, New York.
[61] Fung, Y.-C., 2013, *Biomechanics: Mechanical Properties of Living Tissues*, Springer Science & Business Media, New York.
[62] Wang, Q., Liu, M., Wang, Z., Chen, C., and Wu, J., 2021, "Large Deformation and Instability of Soft Hollow Cylinder With Surface Effects," ASME J. Appl. Mech., **88**(4), p. 041010.